Investigating predictability of offshore winds using a mesoscale model driven by forecast and reanalysis data

Gryning, Sven-Erik; Floors, Rogier

Published in:
Meteorologische Zeitschrift

Link to article, DOI:
10.1127/metz/2019/1002

Publication date:
2020

Document Version
Publisher's PDF, also known as Version of record

Meteorol. Z. (Contrib. Atm. Sci.), Vol. **29**, No. 2, 117–130 (published online February 6, 2020)

Investigating predictability of offshore winds using a mesoscale model driven by forecast and reanalysis data

Sven-Erik Gryning* and Rogier Floors

DTU Wind Energy, Technical University of Denmark, Risø Campus, Roskilde, Denmark

(Manuscript received September 23, 2019; in revised form November 22, 2019; accepted November 25, 2019)

Abstract

The atmosphere is inherently unpredictable by deterministic Numerical Weather Prediction models at both small and large temporal and spatial scales with some intermediate regime where predictability has been demonstrated; this study deals with time scales only. The chaotic nature at the smaller time scales is predominantly caused by turbulence and at the large scales by non-linearity of the Navier-Stokes equations. We investigate, based on observations carried out with a wind-lidar at the FINO3 research platform in the North Sea, the ability of the Weather Research and Forecasting model (WRF) to simulate the changes in the observations ahead of time. The simulations are performed in two ways. In one type the model uses boundary conditions from a reanalysis data-set (WRF-ERA). Alternatively, the simulations are carried out using boundary conditions from a forecast (WRF-GFS). In this study focus is on the predictability of changes in the wind speed and direction. A metric is suggested that chiefly accounts for point-wise changes in the wind speed and direction including turbulent structures. However, for completeness, a traditional metric that compared predicted and observed wind speed and direction directly is also applied. This metric does not reflect the turbulent structures of the flow for small lead times, as the new metric does. The traditional metric reveals very good skills (Fig. 2) up to a lead time of 4 days for simulations in forecast mode (WRF-GFS). By applying the new metric and a correlation coefficient of 0.6 as the lower limit for the skill in the simulations at a height of 126 m, corresponds to a lead time of ≈4 hours (reanalysis) and ≈3 hours (forecast) for both wind speed and direction for turbulence limited lead times. This value is larger than typically found over land – being ≈2 hours. The difference likely relates to the marine conditions of the measurement site. For large lead times, when the simulations are nudged towards the reanalysis the forecast skill does not deteriorate for increasing lead times. This is in contrast to simulations nudged towards meteorological forecasts where the predictability is limited by the non-linearity of the Navier-Stokes equations and a correlation coefficient less than 0.6 was found for lead times larger than ≈6 days for wind speed and somewhat smaller – ≈4 days for the wind direction when applying the new metric. Thus, the window of predictability of the WRF simulations nudged towards a forecast is found to be in the interval ≈4 hours up to ≈6 days (wind speed) and ≈3 hours to ≈4 days (wind direction). These numbers refer to a height of 126 m. The predictive skill is found to be a function of height; at 626 m it is better than at 126 m for both wind speed and direction. For the traditional metric a correlation of less than 0.6 was realized for a lead time larger than ≈4 days for both wind speed and direction.

Keywords: Off-shore, wind-lidar, wind profile, numerical modelling, forecast, reanalysis, lead time

1 Introduction

Because wind resources are highly variable, it is important to be able to assess them accurately to secure a profitable return on the investment in the wind turbines and their efficient and economic integration into the electrical power grid.

Numerical meteorological models are widely used in many applications, but in connection with wind energy the majority of efforts are focused on simulating the wind field in connection with wind resource assessment – so-called analysis – or to forecast the wind conditions ahead of time in connection with energy trading and prediction of hazardous events.

Earlier wind energy assessment studies were typically based on long data-series of meteorological measurements from masts (Troen and Petersen, 1989). This limited the validation to heights of about 100 m (Carvalho et al., 2014; Durante and Westerhellweg, 2012; Floors et al., 2013; Gryning, 1985, Gryning et al., 2007; Steyn and McKendry, 1988; Suomi et al., 2015; Peña et al., 2010, Peña et al., 2015) in most cases although investigations have been carried out based on data from well-instrumented 200–300 m tall masts, e. g. near Hamburg in Germany (Brümmer et al., 2012, Brümmer and Schultze, 2015), Cabauw in the Netherlands (Borsche et al., 2016, van Ulden and Wieringa, 1996) and Østerild in Denmark.

However, reanalysis datasets are being increasingly used as a source for long-term time series of wind values for use in wind energy assessment studies. Reanalysis data sets combine vast amounts of historical obser-

*Corresponding author: Sven-Erik Gryning, DTU Wind Energy, Technical University of Denmark, Risø Campus, Frederiksborgvej 399, 4000 Roskilde, Denmark, e-mail: sveg@dtu.dk

vations into global estimates using modelling and data assimilation systems (Bengtsson and Shukla, 1988; Parker, 2016). Reanalysis data sets are an appealing alternative when direct measurements from meteorological masts are sparse or have limited temporal coverage. However, today reanalysis data have a spatial and temporal resolution which may be adequate for continental scale wind energy resources assessments but are too large for direct use for wind energy purposes e.g. wind farms. Typical spatial and temporal resolutions are 50 km and 6 hours respectively, but large efforts are being put into the establishment of reanalysis data sets with ever increasing spatial and temporal resolutions. Examples of reanalysis data-set are the MERRA (Rienecker et al., 2011), ERA-Interim (Dee et al., 2011), ERA5 (Hersbach and Dee, 2016), and the regional reanalysis COSMO-REA (Bollmeyer et al., 2015).

The highly competitive energy market of today is one of many industries that depend heavily on mesoscale numerical forecast modelling. Numerical forecast models rely on predictions from global forecasts to simulate how the weather most likely evolves out to several days ahead. Global forecasts of meteorological fields are operationally made and archived at a number of large institutions such as European Centre for Medium-Range Weather Forecasts – ECMWF (IFS – Integrated Forecasting System), National Centers for Environmental Prediction – NCEP (GFS – Global Forecast System) and Deutscher Wetterdienst – DWD (ICON – ICOsahedral Nonhydrostatic) just to mention a few. Similarly to the reanalysis products, the global forecasts have spatial and temporal resolutions that in relation to wind energy will require downscaling of the wind field to smaller scales in support of detailed planning of e.g. wind farms.

Downscaling can be performed by Regional Climate Models (RCM) and Empirical Statistical Downscaling (ESD), which are applied over a limited area. In dynamic downscaling, a Regional Climate Model (RCM) is set up for a region of interest and forced at the boundaries by a large scale reanalysis or global forecast data-set. The RCM resolution is usually much higher than the data-set it is nested within and it accounts for the forcing by e.g. complex topographical features and land cover heterogeneities in a physically-based way. There exists a multitude of meso-scale models that have been applied for downscaling e. g. SMHI-RCA4 (Collazo et al., 2018), REMO (Jacob, 2014; Pietikäinen et al., 2018), Arome (Seity et al., 2011), PRECIS (Simmons and Burridge, 1981; Simon et al., 2004), and the Weather Research and Forecasting (WRF) model developed at the National Centre of Atmospheric Research in the United States just to mention a few. In this study, we will apply the WRF model (Skamarock et al., 2008) to downscale the reanalysis or global forecast time-series.

A fundamental problem in Regional Climate Models, as in any numerical weather prediction model, lies in the partial differential equations that need to be supplemented with a large number of parameterizations such as radiation, heat exchange and the effects of terrain which add to the uncertainty of the model predictions. A study of the performance of parameterizations of the model is given in Draxl et al. (2014) where 7 planetary boundary-layer (PBL) schemes are applied and the simulations are compared to one month of meteorological observations at a coastal site in Denmark. Similar exercises (Boadh et al., 2016; Banks et al., 2016) has been reported in the literature for several sites and climate conditions but are often based on short periods and thus do not provide a generally accepted sound guidance on the choice of parameterization schemes to accurately predict winds.

Another fundamental problem is that the atmosphere is inherently chaotic at both the small and the larger time and spatial scales with some intermediate regime where a certain predictability has been demonstrated. In this study only the dependence on the times scales is analysed. The chaotic nature at the smaller time scales is predominantly caused by turbulence and at the larger scales by the limit in predictability, as the accuracy degrades in time due to the non-linear nature of the deterministic Navier-Stokes equations (Lorenz, 1963; Wyngaard, 2010). For very short lead times, statistical models ranging from auto-regression time series models (Pinson, 2012), to more complex models accounting for changes in the dynamical pattern, so-called 'regime switching' models (Pinson et al., 2008) have obtained some success compared to deterministic numerical models with lead times of less than a few hours (Vincent and Trombe, 2017). Haupt et al. (2014) found that the optimal time for switching from statistical to physical modelling occurs beyond 2–3 hours. However, the time scales and the dependence on the atmospheric conditions when physical modelling become superior is not settled and still a matter of discussions and investigations (Vincent and Trombe, 2017).

Therefore, knowledge of the predictive skills of numerical models is essential and it cannot be established without real observations. The limitations in height coverage and the considerable costs of installing and maintaining of meteorological masts, especially off-shore, as well as the urgent need from the wind energy sector for high-resolution accurate observations up to several hundreds of meters, have spurred the development of remote sensing techniques for use in connection with wind energy. Of the many technical efforts, especially Doppler wind lidar has experienced a rapid development and is now beginning to be successfully applied in the renewable energy sector to acquire useful meteorological observations not only of wind-speed and direction, but also wind veer, wind shear and promising efforts to measure turbulence (Sathe and Mann, 2013) and gusts (Suomi et al., 2017) are being attempted.

Based on one year of wind lidar measurements from an off-shore site in the North Sea the ability of the Advanced Weather Research and Forecast model (WRF-ARW) to predict the observed wind speed and -direction is investigated. The WRF simulations are performed in two ways 1) in analysis mode where WRF

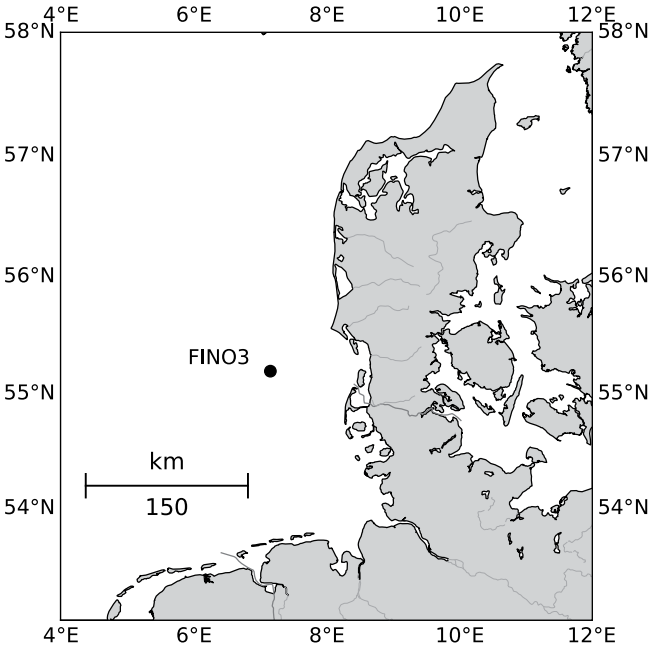

Figure 1: Map showing the position of the observation location, the research platform FINO3. Water is marked in white and land in grey.

is forced with the reanalysis time series of the meteorology (ERA-Interim), and 2) in forecast mode where the WRF simulations are forced with forecasted time-series (GFS). The predictions deal both with the statistical distributions and the ability of the model to predict the conditions for various lead times.

2 Site and Instrumentation

The observations for this study have been collected at the German Research Platform FINO3 (55.19501° N; 7.15836° E) located in the North Sea 80 km west of the Danish island Rømø, Fig. 1, at a water depth of 22 m. A number of off-shore wind farms lie in the near vicinity but the construction of these were not yet initiated during the measuring campaign. The FINO3 platform is equipped with a helicopter deck at 24 m above the mean sea level (msl) as well as a meteorological mast. From 29 August 2013 to 4 October 2014 the measurements were supplemented with a pulsed heterodyne detection Doppler wind lidar – Leosphere WLS70 (Cariou, 2013) – installed on the working platform at 24.5 m. Starting from 100 m above the instrument up to 2 km with a 50 m vertical resolution, horizontal wind velocities are determined. The data were sampled every 30 s and averaged in 10 min mean values. Details on the wind lidar and how it was operated during the campaign are provided by Gryning et al. (2014).

Contrary to measurements by a cup-anemometer, wind speed measurements performed by a wind-lidar are assigned a quality indicator expressed as the Carrier-to-Noise-Ratio (CNR). High values signify more accurate estimates of the wind speed. Following Frehlich (1996), a threshold value of −22 dB is traditionally applied to the wind-speed data series. Gryning et al. (2016) and Gryning and Floors (2019) pointed out some consequence of the choice of a CNR threshold value on the wind observations: increasing the CNR threshold value above the factory threshold value (in the actual case −35 dB) increases the estimated mean wind speed and can affect the wind-rose. The effect was especially pronounced for off-shore observations but was also found over land and in coastal areas. Considering the effect that the filtering with a CNR threshold value can have as discussed above, following the recommendations by Gryning and Floors (2019), the analysis is based on all available observations corresponding to the factory setting of CNR > −35 dB as a threshold value.

Although observations are available for a whole year, the analysis in this study is based on measurements from 29 August to 30 November 2013, partly because the wind-lidar was operating very well during this period (90 % availability at 126 m and 84 % at 626 m), and partly because the numerical simulations in the forecast mode were available for this period only.

3 Numerical Modelling

Wind profiles were simulated using the WRF model (Skamarock et al., 2008) version 3.6. It is a numerical weather prediction and atmospheric simulation system designed for both research and operational applications. The model set-up includes the Noah land-surface scheme (Chen and Dudhia, 2001), the MM5-similarity surface-layer scheme (Zhang and Anthes, 1982), the Thompson microphysics scheme (Thompson et al., 2004), and the 1st-order closure YSU planetary boundary-layer (PBL) scheme (Noh et al., 2003). The level 4 daily sea surface temperature analysis from the Danish Meteorological Institute for the North and Baltic Seas, having a resolution of 0.02°, was used (Høyer and Karagali, 2016).

The WRF model was configured to calculate the meteorological parameters at 70 vertical levels from the surface to the 50 hPa pressure level, 25 of these levels were within the ≈600 m height extent of interest to this study, and the first model level was at 11 m. Three nested domains with a horizontal grid size of 18, 6 and 2 km respectively were used. The time step of the model in the outermost domain was 90 s and decreased with the same ratio as the grid spacing in the inner domains. In order to prevent the model from drifting from the large-scale features of the flow, the model was nudged at the lateral boundaries using linearly interpolated 6 hourly values. Spectral nudging was applied during each model time step for the wind, temperature, and humidity above the 25th model level (approximately corresponding to 600 m), on the outermost model domain during the whole simulation period. Nudging was always switched off in the boundary layer. This nudging set-up was also used in Floors et al. (2018) where more details can be found. The model simulations were

performed in both analysis and forecast mode. Here simulations covering the period 29 August to 30 November 2013 will be analyzed.

3.1 Simulations in analysis mode

In the analysis mode, the model was nudged towards the ERA-Interim Reanalysis (ERA) boundary conditions data available every 6 hours on a $0.7° \times 0.7°$ grid. The simulations were initialized every 10 days at 1200 UTC and after a spin-up of 24 h, a time series of 10 min fields was selected from the simulated meteorological data from 25 to 264 h.

3.2 Simulations in forecast mode

When the model was run in the forecast mode, it was nudged towards the Global Forecast System (GFS), a weather forecast model produced by the NOAA National Centers for Environmental Prediction (NCEP). Forecasts are available every 6 hours on a $0.5° \times 0.5°$ grid. Forecasts with 10 min output were performed every 6 hours up to a forecast horizon of 8 days. It is noted that that the FINO3 observations are not assimilated into the reanalysis nor forecast data.

4 Data analysis

In this section a comparison between observations and the WRF model simulations nudged towards the reanalysis data (WRF-ERA) as well as the GFS forecast data (WRF-GFS) is presented. Finally, an analysis of the similarities and differences in the skills of the WRF-ERA and WRF-GFS model simulations for lead times up to 8 days is presented. All illustrations are shown for a height of 126 m, corresponding to the lowest observation height of the wind lidar and it is also the most relevant for today's wind turbines, however many are also illustrated for 626 m height.

4.1 Lead time analysis

Here the skill of the WRF model to simulate the changes in the observations ahead of time will be discussed. The lead time, Δt, is here defined as the look-ahead time from time t, where t is any time in the discrete series and thus independent of the time of initialization and nudging of the model simulations. The variability of the change of the wind-speed and direction will be investigated for lead times of 10 min to 8 days.

Although the focus in this paper is on the predictability of changes in the wind speed and direction, for completeness, a traditional metric that compares predicted and observed wind speed and direction directly is applied as well. It is based on a comparison of predicted and observed wind speeds, $u_{\mathrm{WRF}}(t+\Delta t)$, $u_{\mathrm{obs}}(t+\Delta t)$, and directions $\mathrm{dir}_{\mathrm{WRF}}(t+\Delta t)$, $\mathrm{dir}_{\mathrm{obs}}(t+\Delta t)$, respectively. This metric is not meant to deal with the influence of atmospheric turbulence. The skill of the comparison between the predictions and observations is traditionally deduced from their Bias, Root Meat Square Error (RMSE) and the correlation coefficient.

Fig. 2 illustrates the skill of the simulations when forced by the ERA reanalysis (upper level) and the GFS forecasts (lower level) for a lead time up to 8 days. It can be seen that for short lead times, the skills are somewhat similar; corresponding to a bias of $\approx 0.4\,\mathrm{m\,s^{-1}}$ and $\approx 4°$ for wind speed and direction and the corresponding RMSE values are $\approx 2\,\mathrm{m\,s^{-1}}$ and $\approx 20°$ respectively. This shows that the WRF for this set of observations predicts very well the general wind conditions for short lead times, but not the effect of turbulence in the observations

The main focus in this paper is on the predictability of changes in the speed and direction. A metric is suggested that is based on the individual differences in wind speeds $\Delta u(\Delta t)$ and wind direction $\Delta\mathrm{dir}(\Delta t)$ between $t+\Delta t$ and t where t is time and Δt is the lead time:

$$\Delta u_{\mathrm{obs}}(\Delta t) = u_{\mathrm{obs}}(t+\Delta t) - u_{\mathrm{obs}}(t) \tag{4.1}$$

$$\Delta\mathrm{dir}_{\mathrm{obs}}(\Delta t) = \mathrm{dir}_{\mathrm{obs}}(t+\Delta t) - \mathrm{dir}_{\mathrm{obs}}(t) \tag{4.2}$$

where subscript *obs* denotes observations; correspondingly for the WRF simulations

$$\Delta u_{\mathrm{WRF}}(\Delta t) = u_{\mathrm{WRF}}(t+\Delta t) - u_{\mathrm{WRF}}(t) \tag{4.3}$$

$$\Delta\mathrm{dir}_{\mathrm{WRF}}(\Delta t) = \mathrm{dir}_{\mathrm{WRF}}(t+\Delta t) - \mathrm{dir}_{\mathrm{WRF}}(t) \tag{4.4}$$

where subscript *WRF* denotes the model simulations. Time series were derived for Δt ranging from 10 min to 8 days. The skill of the numerical model to simulate the changes to the wind field will be assessed from the difference in concurrent individual observed and the predicted changes of the wind speed $\delta u(\Delta t)$ and direction $\delta\mathrm{dir}(\Delta t)$:

$$\delta u(\Delta t) = \Delta u_{\mathrm{obs}}(\Delta t) - \Delta u_{\mathrm{WRF}}(\Delta t) \tag{4.5}$$

$$\delta\mathrm{dir}(\Delta t) = \Delta\mathrm{dir}_{\mathrm{obs}}(\Delta t) - \Delta\mathrm{dir}_{\mathrm{WRF}}(\Delta t). \tag{4.6}$$

4.2 Examples of wind speed and direction change histograms for various lead times

To illustrate the lead time dependence, examples of histograms of the wind-speed $\Delta u_{\mathrm{obs}}(\Delta t)$, $\Delta u_{\mathrm{WRF}}(\Delta t)$ and $\delta u(\Delta t)$, and similarly for the wind-direction are shown for lead times of 10 min, 24 hours and 7 days. By comparing the distributions, the effect of the 3 fundamental stages (turbulence limited, skilled prediction, limited by non-linear interactions) in the predictability of numerical models is illustrated.

Fig. 3 shows the distribution of wind speed changes for lead times of 10 min, 24 hours and 7 days represented by histograms. The upper rows are WRF-ERA and the lower rows are WRF-GFS simulations. In the left panels (lead time 10 min) it can be seen that the distribution of the wind speed change observations by the lidar and the distribution of the difference between the lidar observations and the WRF simulated wind speeds changes are almost identical, but the WRF predictions have a much

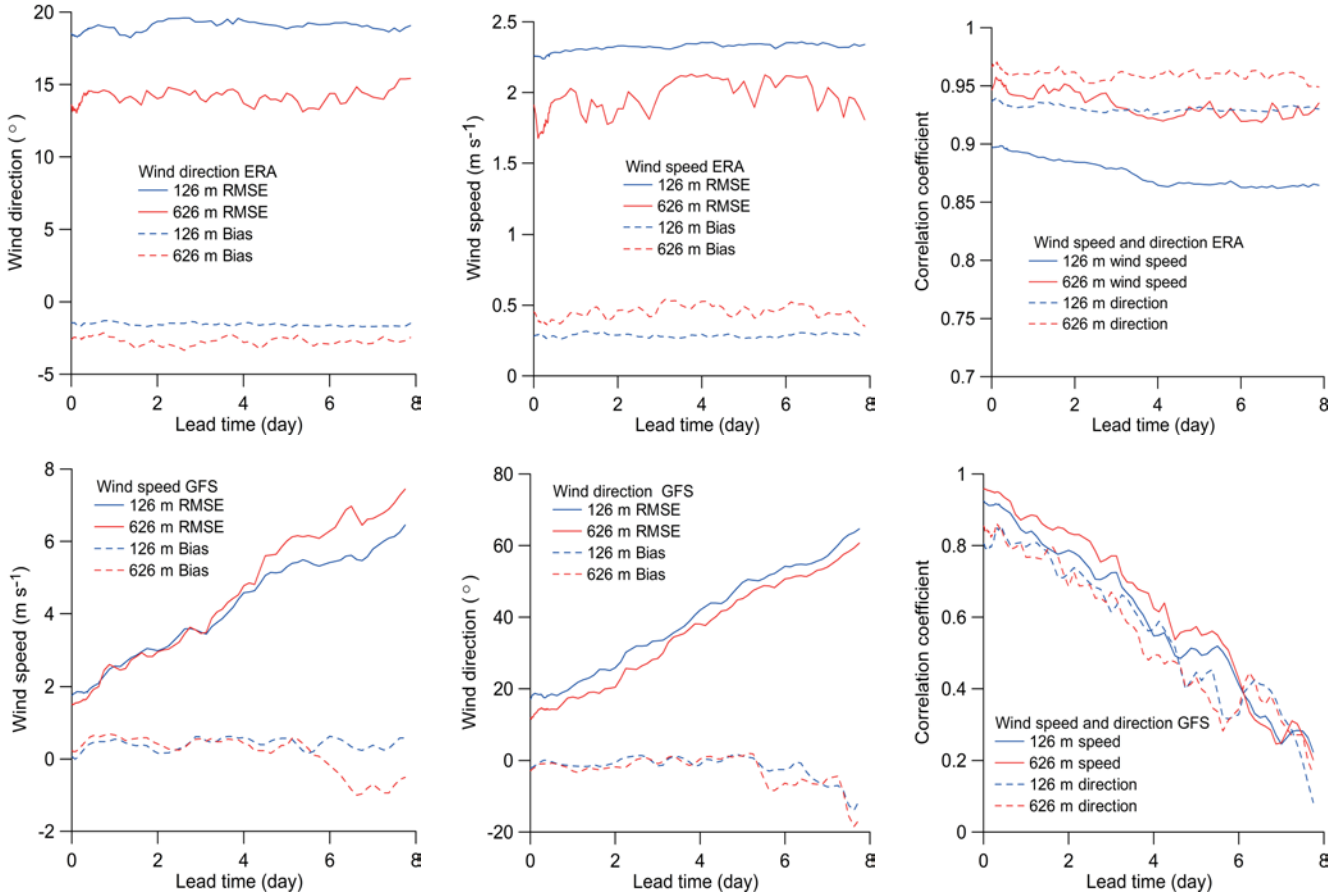

Figure 2: Bias and Root-Mean-Square-Error (RMSE) for wind speed (left panels), same for wind direction (middle panels) and correlations coefficients for both wind speed and direction (right panels) as function of the lead time when applying the traditional metric: $Bias_u = \frac{1}{N}\sum_{i=1}^{N}(u_{\mathrm{obs}}(t+\Delta t) - u_{\mathrm{WRF}}(t+\Delta t))$; $RMSE_u = (\frac{1}{N}\sum_{i=1}^{N}(u_{\mathrm{obs}}(t+\Delta t) - u_{\mathrm{WRF}}(t+\Delta t))^2)^{0.5}$. Here the metric is shown for the wind speed but it is similar for the wind direction. Upper panels represent WRF-ERA, lower panels WRF-GFS.

narrower distribution. The latter indicates that WRF is unable to predict the turbulent fluctuations in the wind speed for a lead time of 10 min.

This pattern is altered in the middle panels, representing lead times of 24 hours. Here the distribution of the lidar observations and the WRF simulated wind speed changes are nearly equal; and the distribution of the difference between the lidar observations and the WRF simulated wind speeds is narrow compared to those of the lidar and WRF, indicating that WRF for a lead time of 24 hours has gained predictive skills.

This pattern is characteristic for both the WRF simulations performed in analysis mode i.e. nudged towards ERA-Interim analysis, and for simulations in the forecast mode nudged towards GFS. However for a lead time of 7 days, illustrated in the right panels of Fig. 3, the non-linear nature of the WRF-GFS simulations comes into play and the pattern becomes different for the two simulations. For the simulations in analysis mode (WRF-ERA), the predictive ability of the WRF simulations remains largely unaltered, but this is not the case for the forecasts based on WRF-GFS. Here the 3 distributions resemble each other indicating low skills in forecasting changes in the wind speed.

Similarly, Fig. 4 shows the ability of WRF to predict changes in wind direction, and the same overall pattern is found.

4.3 Predictive skill as a function of lead time

In order to investigate the predictive ability in further detail and taking the wind speed as an example, it can be noted that $\delta u(\Delta t)$ is composed as a difference of two statistical distributions, that of $\Delta u_{\mathrm{obs}}(\Delta t)$ and of $\Delta u_{\mathrm{WRF}}(\Delta t)$. From a statistical point of view, the distribution of the differences of two normally distributed variables with variances σ_x^2 and σ_y^2 is another normal distribution with variance $\sigma_{\mathrm{total}}^2$ where

$$\sigma_{\mathrm{total}}^2 = \sigma_x^2 + \sigma_y^2 - 2\rho\sigma_x\sigma_y \tag{4.7}$$

provided that the two variables are correlated with a correlation coefficient of ρ. In our case Eq. (4.7) can be written:

$$\sigma^2(\delta u(\Delta t)) = \sigma^2(\Delta u_{\mathrm{obs}}(\Delta t)) + \sigma^2(\Delta u_{\mathrm{WRF}}(\Delta t)) - 2\rho\sigma(\Delta u_{\mathrm{obs}}(\Delta t))\sigma(\Delta u_{\mathrm{WRF}}(\Delta t)) \tag{4.8}$$

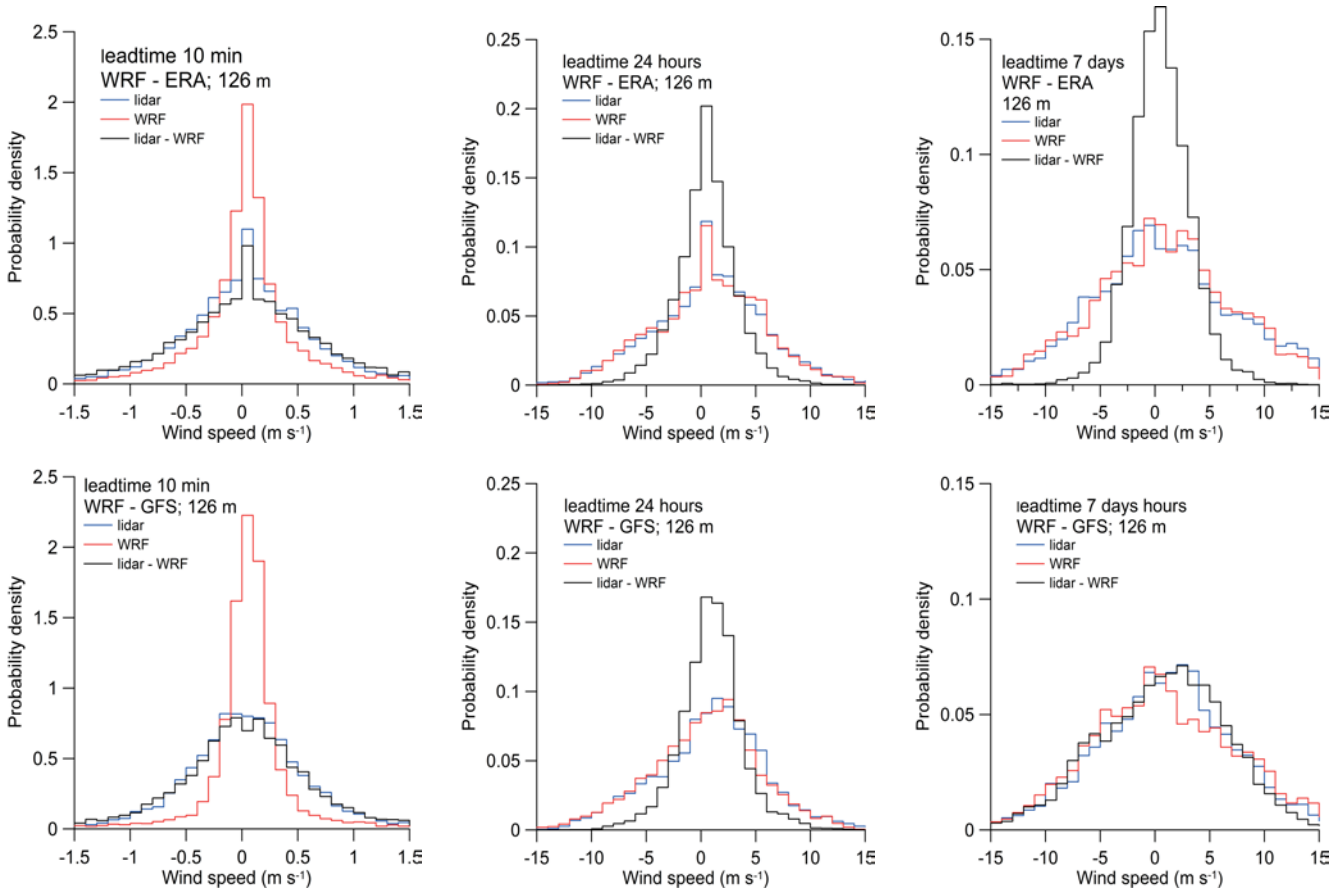

Figure 3: Distributions of wind speed change for a lead time of 10 min (left panels), 24 hours (middle panels) and 7 days (right panels). The blue lines are the observations, $\Delta u_{\mathrm{obs}}(\Delta t)$, the red lines the simulations $\Delta u_{\mathrm{WRF}}(\Delta t)$ and the black lines $\delta u(\Delta t)$. The upper panels illustrate the WRF-ERA simulations, the lower panels the WRF-GFS. The results are illustrated for the 126-m height.

$$\sigma^2(\delta\mathrm{dir}(\Delta t)) = \sigma^2(\Delta\mathrm{dir}_{\mathrm{obs}}(\Delta t)) + \sigma^2(\Delta\mathrm{dir}_{\mathrm{WRF}}(\Delta t)) - 2\rho\sigma(\Delta\mathrm{dir}_{\mathrm{obs}}(\Delta t))\sigma(\Delta\mathrm{dir}_{\mathrm{WRF}}(\Delta t)) \tag{4.9}$$

The behavior of Eqs. (4.8) and (4.9) can be written as

$$\sqrt{\frac{\sigma^2(\delta u(\Delta t))}{\sigma^2(\Delta u_{\mathrm{obs}}(\Delta t)) + \sigma^2(\Delta u_{\mathrm{WRF}}(\Delta t))}} \leq 1 \tag{4.10}$$

$$\sqrt{\frac{\sigma^2(\delta\mathrm{dir}(\Delta t))}{\sigma^2(\Delta\mathrm{dir}_{\mathrm{obs}}(\Delta t)) + \sigma^2(\Delta\mathrm{dir}_{\mathrm{WRF}}(\Delta t))}} \leq 1 \tag{4.11}$$

when the observations are positively correlated with the simulations. The left-hand-side of Eqs. (4.10) and (4.11) will decrease with an increasing ability of the simulations to predict the observations. The ultimate goal for the numerical prediction is, of course, a perfect agreement between observations and simulations which corresponds to a variance of zero for the distribution of $\delta u(\Delta t)$ and $\delta\mathrm{dir}(\Delta t)$. From the right-hand-side of Eqs. (4.8) and (4.9) it can be seen that it is not a sufficient condition for perfect agreement that the correlation coefficient is one for both wind speed and direction but also that the variances of the observations and the model predictions are equal, i.e. $\sigma(\Delta u_{\mathrm{obs}}(\Delta t)) = \sigma(\Delta u_{\mathrm{WRF}}(\Delta t))$ and $\sigma(\Delta\mathrm{dir}_{\mathrm{obs}}(\Delta t)) = \sigma(\Delta\mathrm{dir}_{\mathrm{WRF}}(\Delta t))$.

It can be noted that agreement between the distributions of $\Delta u_{\mathrm{obs}}(\Delta t)$ and of $\Delta u_{\mathrm{WRF}}(\Delta t)$ does not indicate that the predictive skill of the numerical simulation is good, nor does a correlation coefficient close to one. The two must be interpreted in combination.

How long a lead time is required before the simulations of the changes in wind speed and direction acquire some skill? For the WRF-ERA simulations, this is illustrated in Fig. 5. It can be seen that for small lead times the left-hand-side (l.h.s.) of Eqs. (4.10) and (4.11) are close to one, indicating that the observations are poorly correlated with the numerical simulations. That the model skill being small at shorter lead times is a reflection of the fact that a mesoscale model does not reproduce turbulent motions, which the observations include. This applies for both the wind speed and direction. This behavior is also reflected in the correlation coefficient (Fig. 5 right panel) being close to zero for small lead times, then increasing as the lead time increases. Because the simulations are nudged towards reanalysis data and thus take advantage of measurements ahead of time, the skill does not deteriorate as the lead time increases. The normalized variance remains at a value of about ≈ 0.4 for the wind speed and ≈ 0.3 for the direction

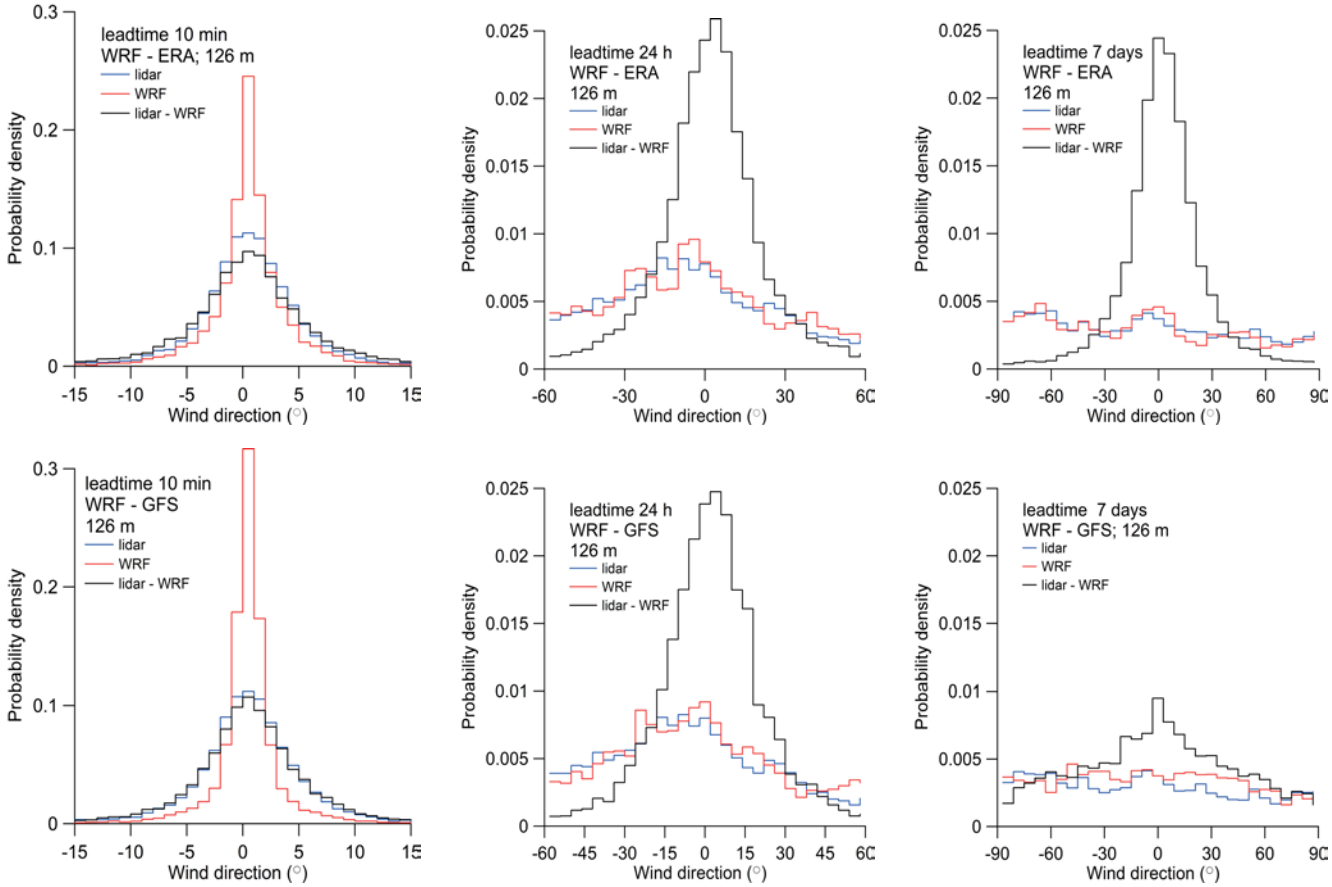

Figure 4: As for Fig. 3 but for wind direction.

at the 126 m height; the corresponding correlation coefficients being ≈ 0.8. Taking, as suggested by Hollingworth et al. (1980), a correlation coefficient of 0.6 as a the lower limit for skills in the simulations, corresponds to a lead time of ≈ 5 hours for wind speed and ≈ 4 hours for the direction at 126 m. The skills in the simulations can be seen to be represented by a smaller lead time for the wind speed at 626 m as compared to 126 m, being ≈ 3.5 hours and similarily for both wind speed and direction, with a higher correlation coefficient of ≈ 0.9.

For the simulations in forecast mode, WRF-GFS, that are nudged towards the GFS forecasts and therefore do not take advantage of the measured meteorological conditions ahead of time, as is the case for the reanalysis data, but solely relying on forecasted data, the behavior is shown in Fig. 6. For small lead times, the normalized variances are close to one and the correlation coefficients are near zero for both wind speed and direction, indicating very little skills. This behavior resembles the conditions from the reanalysis simulations in Fig. 5. Following this stage, skills in the simulations are obtained corresponding to a normalized variance of ≈ 0.4 for wind speed and ≈ 0.3 for direction at 126 m, and the corresponding correlation coefficient are slightly less than ≈ 0.9, being lower for the wind speed. These conditions remain near constant up to a lead time of 3 days, followed by a gradual increase of the normalized variances and a corresponding decrease of the correlation coefficient. This general behavior continues up to a lead time of 8 days, corresponding to the maximum length of the simulations. Even for a lead time of 8 days the simulations exhibit skill corresponding to a normalized variance of 0.7 and 0.6 for wind speed and direction, respectively, with the corresponding correlation coefficients being ≈ 0.4. Taking the correlation coefficient of 0.6 as a lower limit for predictions with some skill, the WRF-GFS simulations have skills for lead times in the interval ≈ 3.5 hours to 6 days for the wind speed, and the corresponding values for the wind direction are 3 hours to 4 days respectively at 126 m. The predictive skills for both wind speed and direction are in general better at 626 m height than at 126 m. Therefore skillful predictions, corresponding to a correlation coefficient larger than 0.6, are obtained for a lead time in the interval ≈ 3.5 hours to ≈ 6 days, and ≈ 3 hours to ≈ 4 days for the wind speed and direction, respectively. It can be noted that even for a lead time of 8 days, predictive skills corresponding to a correlation coefficient of ≈ 0.4 can be observed.

5 Persistence

In the persistence model, the expected value of the parameter ahead of time is assumed to be equal to the most recent value, or that the conditions at the time of the

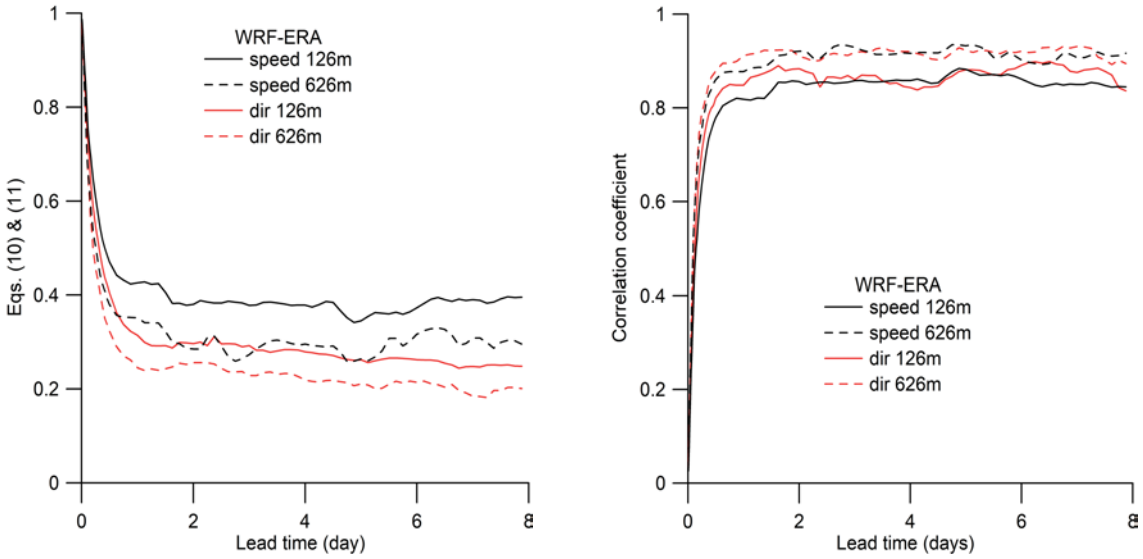

Figure 5: Results from the comparison of observations with WRF-ERA simulations. The normalized variances $\sqrt{\sigma^2(\delta u(\Delta t))/(\sigma^2(\Delta u_{\rm obs}(\Delta t)) + \sigma^2(\Delta u_{\rm WRF}(\Delta t)))}$ (see Eq. (4.10)) and $\sqrt{\sigma^2(\delta dir(\Delta t))/(\sigma^2(\Delta {\rm dir}_{\rm obs}(\Delta t)) + \sigma^2(\Delta {\rm dir}_{\rm WRF}(\Delta t)))}$ (see Eq. (4.11)) are illustrated in the left panel, and the correlation coefficients $\rho(\delta u_{\rm obs}(\Delta t), \delta u_{\rm WRF}(\Delta t))$ and $\rho(\delta {\rm dir}_{\rm obs}(\Delta t), \delta {\rm dir}_{\rm WRF}(\Delta t))$ in the right panel, both as a functions of lead time. Full lines represent 126 m and dashed lines 626 m height; black lines show wind speed and red lines wind direction.

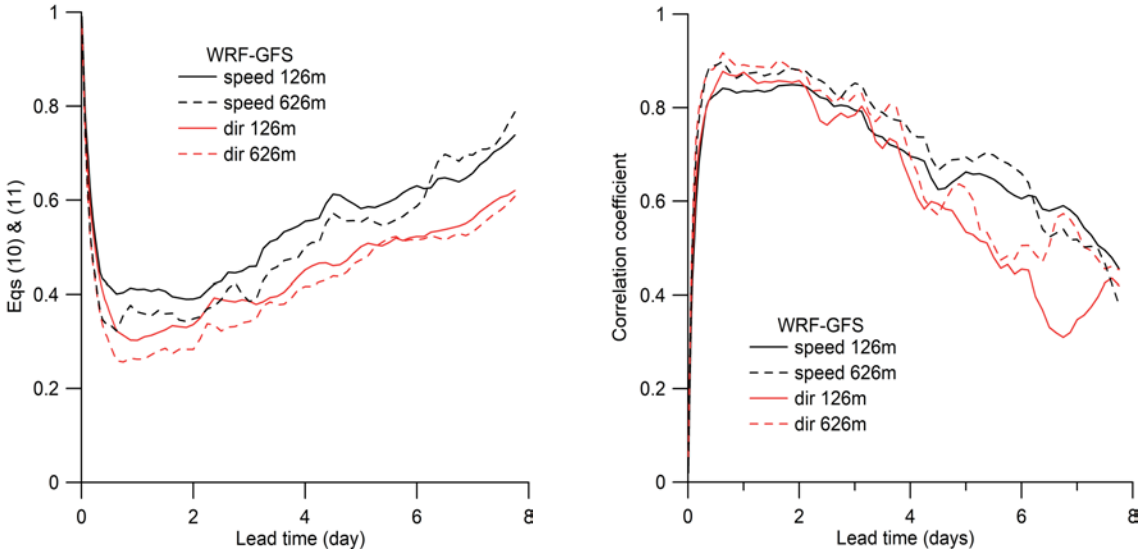

Figure 6: As in Fig. 5 but for WRF-GFS.

forecast will not change. The persistence model is the simplest way of producing a forecast, and it is often used as a reference for many other meteorological models. At very short time scales it is difficult to beat a persistence forecast, however as the lead time increases, changes in wind occur and models with predictability become superior. Here we investigate the lead time where the persistence model is outperformed by predictive models – in this case by the WRF-ERA and WRF-GFS numerical models. The forecast in the persistence model is simply

$$u_{\rm forecast}(t + \Delta t) = u_{\rm obs}(t) \tag{5.1}$$

$$\mathrm{dir}_{\rm forecast}(t + \Delta t) = \mathrm{dir}_{\rm obs}(t) \tag{5.2}$$

This corresponds to that the expected value of the parameter Δt ahead of time is equal to the most recent value. This is obviously a very naive but often very powerful model for short time predictions because the atmosphere statistically changes slowly, i. e. is quasi-stationary. The comparison between the persistence model and any other forecast model is usually done by comparing the RMSE (Root-Mean-Square-Error) of the model predictions. For the persistence model it is

$$RMSE_{u,\rm persistence} = \left(\frac{1}{N} \sum_{i=1}^{N} (u_{\rm obs}(t + \Delta t) - u_{\rm obs}(t))^2 \right)^{0.5} \tag{5.3}$$

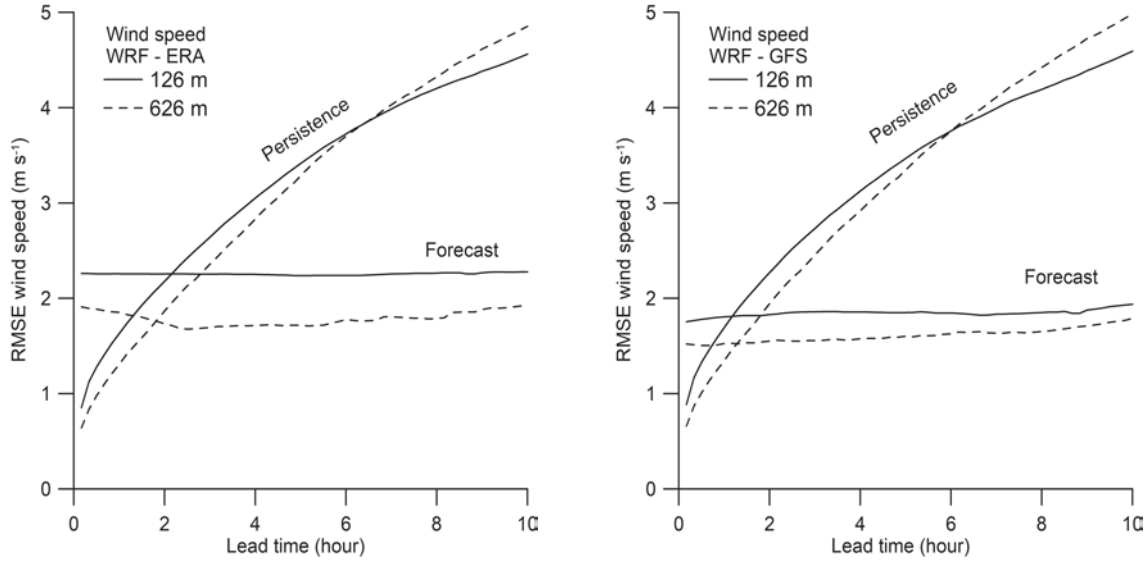

Figure 7: Root-Mean-Square-Error of the wind speed as function of the lead time for the Persistence model $RMSE_{u,\text{persistence}}$ and forecast $RMSE_{u,\text{WRF}}$ for the WRF-ERA (left panel) and the WRF-GFS model simulations (right panel). Full lines illustrate 126 m and dashed lines 626 m height.

$$RMSEr_{\text{dir,persistence}} = \left(\frac{1}{N}\sum_{i=1}^{N}(\text{dir}_{\text{obs}}(t+\Delta t) - \text{dir}_{\text{obs}}(t))^2\right)^{0.5} \quad (5.4)$$

and for this study, wherein the simulations are performed by the WRF model, this will be compared to

$$RMSE_{u,\text{WRF}} = \left(\frac{1}{N}\sum_{i=1}^{N}(u_{\text{obs}}(t+\Delta t) - u_{\text{WRF}}(t+\Delta t))^2\right)^{0.5} \quad (5.5)$$

$$RMSEr_{\text{dir,WRF}} = \left(\frac{1}{N}\sum_{i=1}^{N}(\text{dir}_{\text{obs}}(t+\Delta t) - \text{dir}_{\text{WRF}}(t+\Delta t))^2\right)^{0.5} \quad (5.6)$$

where N is the number of samples. Owing to the atmospheric turbulence and the quasi-stationarity of the atmosphere, $RMSE_{u,\text{persistence}}$ and $RMSE_{\text{dir},persistence}$ will be small for small Δt and will grow as Δt increases. This is in contrast to the WRF predictions $RMSE_{u,\text{WRF}}$ and $RMSE_{\text{dir,WRF}}$, where the lack of ability to simulate the turbulence results in an enhancement of $RMSE_{u,\text{WRF}}$ and $RMSE_{\text{dir,WRF}}$ when Δt is small.

This behavior can be observed in Fig. 7. The left panel illustrates the behavior of $RMSE_{u,\text{persistence}}$ and $RMSE_{u,\text{WRF}}$ for the wind speed predictions at 126 m and 626 m. It can be seen that lead time, for which the persistence model is superior, is ≈ 2 hours for WRF-ERA and a little smaller, ≈ 1.5 h for WRF-GFS. There is little sensitivity to height. For the wind direction, Fig. 8, the lead time for the superiority of persistence is ≈ 1.5 hours for both WRF-ERA and WRF-GFS.

6 Effect of time-shift in the simulations

It is often argued that the agreement between observations and model simulations is affected by a time offset in the simulations. The simulations might be in very good agreement with the observations if they are shifted for some of the simulations. This, of course, hampers the metrics that are used to evaluate the comparison between model simulation and real observations. In order to analyze the issue of a time offset, comparisons were performed for model simulations that have been shifted in time relative to the observations. Sensitivity to offsets in the simulated wind speed and direction depends on the length of the time series that are compared. Here the analysis is based on 24 hour time series that are taken from the total 3 months of available data. A new 24 hour time slice was derived by shifting the observations by 10 min resulting in ≈ 13000 data series of a length of 24 hours. The quality of the agreement between observations and simulations with and without time shifts was evaluated using the following metrics: MAE (Mean Absolute Error), RMSE (Root Mean Square Error) and the correlation coefficient. Figs. 9 and 10 show results that are based on the correlation coefficient but almost similar results were obtained when either MAE or RMSE were used as metrics. Figs. 9 and 10 (left panels) illustrate that with respect to the WRF-ERA simulations a 10 min shift in the simulations provides a better agreement in ≈ 50 % of the cases but a shift of −2 hours only in 20 % of the cases, and a shift of 2 hours in about 30 % of the cases. A zero shift of course corresponds to 100 %. It can be noted that the curves are not symmetric around zero but remain higher for positive time shifts as compared to negative shifts, implying that the comparison is more sensitive to negative than positive shifts of time in the simulated wind field. The

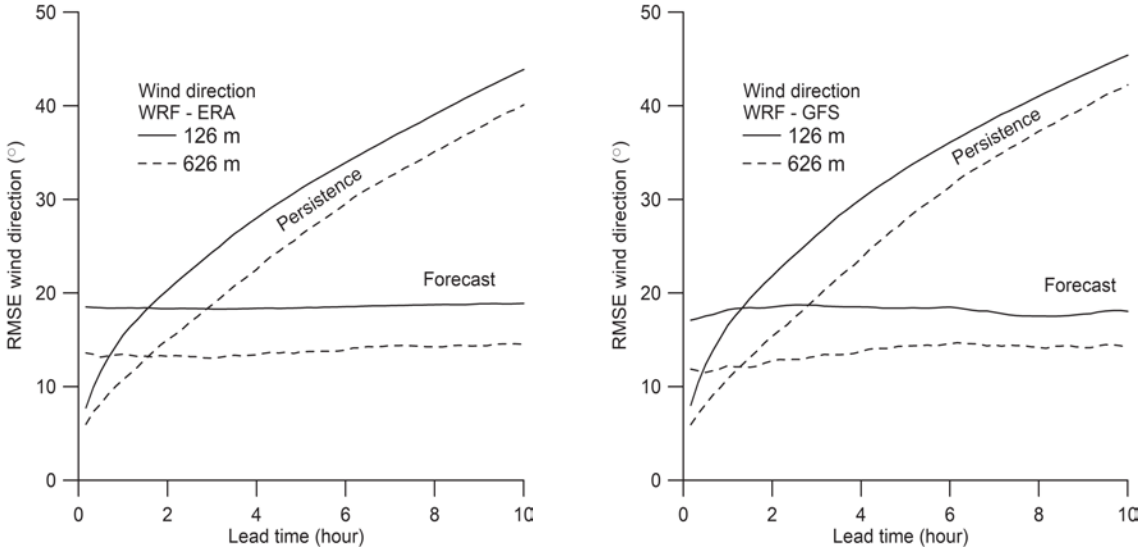

Figure 8: Root-Mean-Square-Error of the wind direction prediction as function of the lead time for the Persistence model $RMSE_{\mathrm{dir,persistence}}$ and forecast $RMSE_{\mathrm{dir,WRF}}$ for the WRF-ERA (left panel) and the WRF-GFS model simulations (right panel). Full lines illustrate 126 m and dashed lines 626 m height.

sensitivity to the time shifts in the simulations for wind speed and wind direction are largely similar.

A similar analysis was performed for the WRF-GFS simulations but in this case an additional parameter emerges. The results will depend on the forecast length in such a way that for a short forecast horizon, e. g. 0.5 day, the result will resemble the WRF-ERA (which is updated every 6 hours) but will differ for large forecast horizons. This effect is shown in Figs. 9 and 10 (right panels) for forecast horizons of 0.5, 2 and 4 days. For the forecast horizon of 0.5 days slightly less than 50 % of the simulations agree better with the observations when a ±10 min shift in time is applied to the simulations. For a time shift of −2 hours this number is reduced to 20 % for both wind speed and direction, and for a time shift of 2 hours the numbers are ≈ 25 % for the wind speed and somewhat lower, ≈ 20 % for wind direction. The overall pattern with high values for small lead times and small values for larger lead times can be observed for a forecast horizon of 2 and 4 days as well, but the likelihood for agreement for a shifted time-series for large lead times is shifted towards higher values. It can be noted that for a forecast horizon of 4 days the dependence on the lead time is small in such a way that in about 50 % of the cases the statistics for a shift in the lead time of the simulations is near the same for both small and large lead times; the curve is almost flat for both wind speed and direction.

7 Discussion

For wind-energy assessment studies, it is important that the overall statistics of the performance of the model resemble the statistics of the observations, and it is less important if the model actually predicts the individual observations. This can be evaluated in terms of their probability distribution functions or the accumulated distribution functions. An example of this type of validation is the continuous ranked probability score (CRPS), which is a commonly used verification index that compares modelled data with the observations, where both are represented as cumulative distribution functions (Hersbach, 2002). Comparing two cumulative distributions, however does not provide information on the skill of the model to predict the individual observations – only on the common statistics.

In order to investigate this further, a point comparison between observations and WRF simulations was performed based on three months of measurements of the wind profile in a windy climate at a marine site in the North Sea. The measurements were carried out with a ∼600 m range wind Doppler lidar in combination with a 100 m tall meteorological mast. Gryning et al. (2016) and Gryning and Floors (2019) show that filtering the observations with a Carrier-to-Noise-Ratio (CNR) threshold value acts as a rather smooth filter that basically shifts the probability distribution of the observations of the wind speed towards higher values which results in a selection of higher wind speeds and a shift in the wind rose compared to the value when all data are used. This means that applying a high CNR threshold value biases the climatology of wind profiles. Therefore in this study, a CNR filtering threshold has not been applied to the measurements. All available observations from the lidar were applied with due respect to missing observations owing to instrument malfunctioning or CNR threshold values falling below the −35 dB factory setting.

The results of the model simulations depend on the choice of the parameterizations of the model as well as the frequency of initialization and nudging of the reanalysis data. The comparison in this part of the study illustrates how well the analysis adapts to the observa-

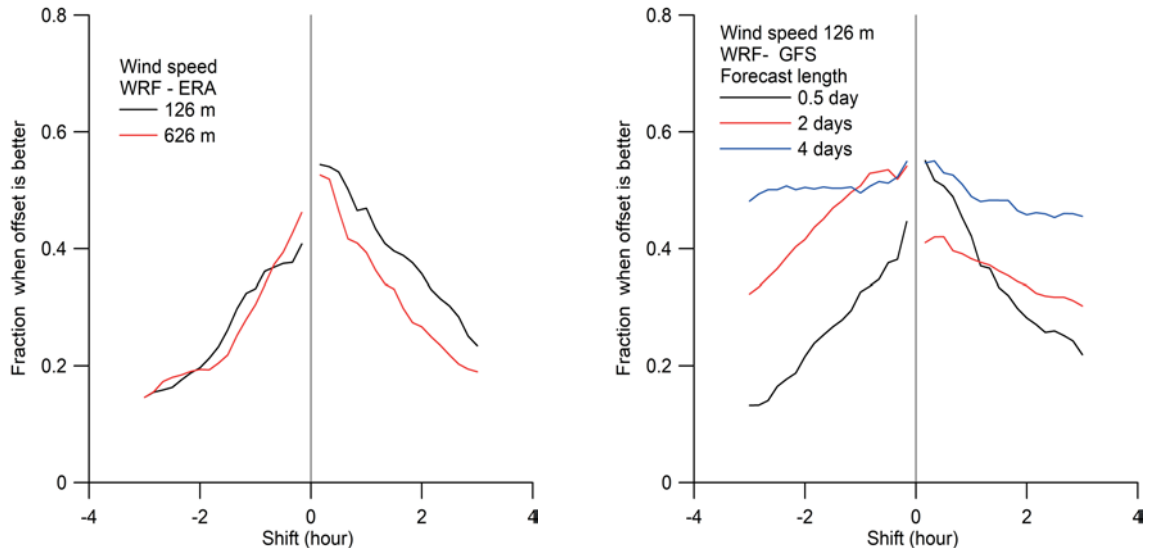

Figure 9: Illustration of the fraction of time that a time-shift in the model simulations of the wind speed improves the correlation with observations. In the left panel, which shows the results for simulations with WRF-ERA, the black line represents a height of 126 m and the red line 626 m. The right panel shows the result of simulations by WRF-GFS at 126 m. Because WRF-GFS represents a true forecast, the results are dependent on the forecast horizon – a forecast horizon of 12 hours (solid black line), 2 days (red line) and blue line (4 days), respectively. A positive phase shift means that the simulations are shifted forward in time (i.e. an observation at 12:00 is compared to simulations at 10:00).

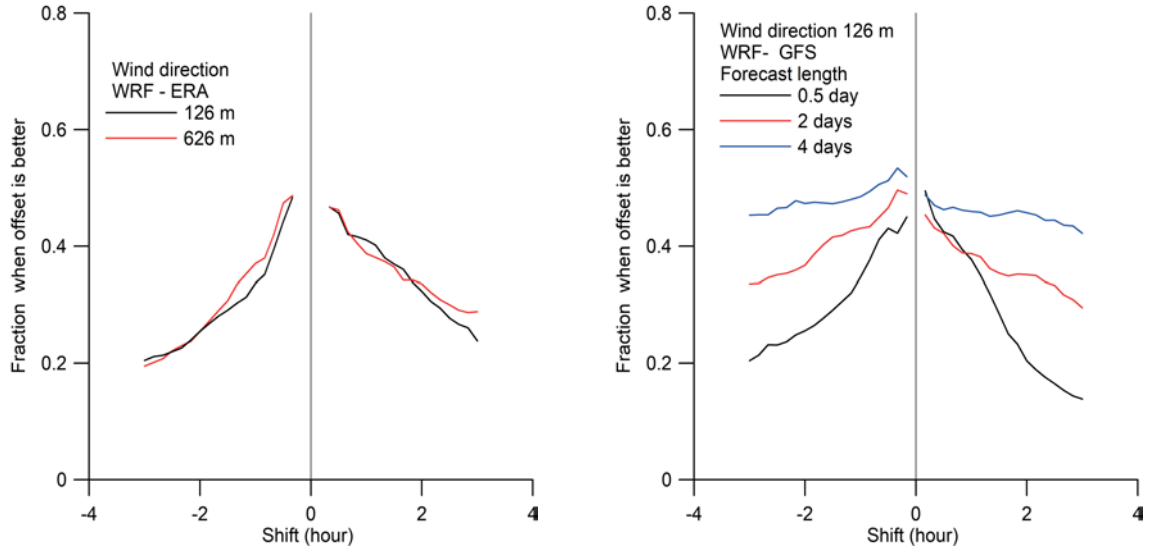

Figure 10: As for Fig. 9 but for wind direction.

tions and does not deal with the ability to forecast the wind field. This is in contrast to the WRF simulations in the forecast mode when the model is driven by a meteorological forecast. In this study, the Global Forecast System (GFS) is used. In both cases, the output depends on the chosen parametrizations of WRF as well as the nudging frequency of the reanalysis or forecasts data respectively. Studies exists, based on short-term time series of observations, on the choice of parameterizations for WRF, but a generally accepted recommendation has not been reached. A comprehensive study, although it would be very useful, on the sensitivity of the large number of reanalysis and forecast data-sets to the WRF model output is still missing due to the huge requirements for computer resources that go far beyond what is available at our institution. The effect on the predictions on the choice of reanalysis or forecast data-set is presently largely not investigated.

When the skill of the simulations was investigated with a traditional metric, that reflects the ability to predict wind speed and direction, the agreement for small lead times (minutes and hours) is very good (see Fig. 2). The limit of predictability for simulations in the forecast mode (forced with GFS) was found to be ≈ 4 days, corresponding to a correlation coefficient of 0.6.

When applying a metric that chiefly emphasizes the changes in the wind speed and direction, the skill of the WRF model was investigated by calculating the normal-

ized RMSE of the observed minus WRF model wind speeds and directions, $\sigma(\delta u(\Delta t))$ and $\sigma(\delta \mathrm{dir}(\Delta t))$ respectively for various lead times Δt, see also Eqs. (4.10) and (4.11). It can be noted that the skill of the simulations increase as the ratio decreases. The simulation skill was also quantified in terms of the Pearson correlation coefficients, $(\rho(\Delta u_{\mathrm{obs}}(\Delta t), \Delta u_{\mathrm{WRF}}(\Delta t))$ and $\rho(\Delta \mathrm{dir}_{\mathrm{obs}}(\Delta t), \Delta \mathrm{dir}_{\mathrm{WRF}}(\Delta t))$ respectively. It can be noted that $\rho > 0$ for all lead times both for wind speed and direction. In agreement with Hollingworth et al. (1989) a correlation coefficient of $\rho = 0.6$ was taken as a lower limit for useful or skilled predictions. It should be emphasized however that the use of RMSE and correlation coefficient in terms of model verification are fundamentally different. While the correlation coefficient is insensitive to any bias and scale differences in the observed and simulated distributions, this is not the case for the RMSE.

For the WRF simulations nudged with the reanalysis data, the corresponding lead time ($\rho = 0.6$) was found to be ≈ 5 hours for the wind speed at 126 m. This value is twice higher than suggested by Haupt et al. (2014). It can be seen from Fig. 5 that the simulation skill improves with increasing lead times, levelling off and reaching a correlation coefficient of ≈ 0.8 for a lead time of ≈ 15 hours and ≈ 11 hours at 126 m for wind speed and direction respectively and somewhat lower, ≈ 7 hours at 626 m. The reason that the correlation coefficient levels off is connected to the 6-hourly nudging of the WRF model simulations with reanalysis data.

In the forecast mode (WRF nudged with GFS), the behaviour of the wind speed and direction is nearly the same. A correlation coefficient of 0.6 is reached at ≈ 3 hours and a correlation coefficient of ≈ 0.8 after ≈ 8 hours at 126 m and ≈ 5 hours at 626 m. In forecast mode, the forecast skill decreases in response to the lack of predictability of the atmosphere due to its nonlinear nature (Lorenz, 1963), reaching a correlation coefficient of 0.6 after ≈ 4 days for the wind speed and somewhat longer, ≈ 6 days for the wind direction.

The persistence approach, which is a commonly used benchmark, (Nielsen et al., 1998), is shown here for completeness. It was found that the persistence model provides better performance compared to the numerical simulations for lead times less than about 2 hours for both wind speed and direction and is twice as large as the value reported (Fig. 1) in Haupt et al. (2014). It can be noted that a persistence time of ≈ 2 hours corresponds to a correlation coefficient of about 0.4 (Figs. 5 and 6) between the changes in the observed and simulated wind speed and direction $(\rho(\Delta u_{\mathrm{obs}}(\Delta t), \Delta u_{\mathrm{WRF}}(\Delta t))$ and $\rho(\Delta \mathrm{dir}_{\mathrm{obs}}(\Delta t), \Delta \mathrm{dir}_{\mathrm{WRF}}(\Delta t))$ respectively for both heights.

The results in this study will be specific for the synoptic conditions in the North Sea which are dominated by the westerlies with frequently passing low pressure systems alternating with fewer more extended periods of high pressure. The outcome of the study reflects the conditions in a marine atmosphere that is adjusted to the sea surface with minor diurnal variation of the temperature. The diurnal variation of the meteorological conditions which are characteristic for over-land conditions is much reduced over the sea (Gryning and Batchvarova, 2002). Variability of the meteorological conditions in the marine atmosphere is more controlled by the prevailing synoptic conditions at the site. It can be speculated that the critical lead times depend on the actual meteorological conditions and over land will be shorter due to the pronounced diurnal variation.

Table 1: WRF cannot capture short-term changes in wind speed and direction caused by turbulent structures. Below is given characteristic lead times to achieve skills corresponding to a correlation coefficient of 0.6. The numbers are based on a comparison between point-wise changes as function of lead time in wind speed and direction.

	WRF-ERA		WRF-GFS	
Height	126 m	626 m	126 m	626 m
Wind speed lead time (hour)	5	3.5	3.5	2.5
Wind direction lead time (hour)	4	3.5	3	2.5

8 Main conclusions

In this study, the focus is on a comparison of the contemporary observed and simulated data, as well as the ability of the numerical model to simulate the changes in the wind conditions ahead of time. The simulations were performed with the WRF model in the long-term analysis mode (WRF-ERA) and the forecast mode (WRF-GFS). In the former case, the model was initialized every 10 days and nudged towards the ERA-Interim boundary conditions every 6 hours.

Based on 3 months of wind-lidar observations over the North Sea the skill of the WRF model to simulate changes in the wind speed and direction was investigated.

When using a metric that emphasizes wind speed and direction the WRF model was found to predict the wind speed and direction with a correlation coefficient ≈ 0.9 (see Fig. 2) for small lead times (minutes to hours), and lack of skills in the forecast mode is found for lead times larger than ≈ 4 days.

Applying a metric that emphasizes the change in wind speed and direction between contemporary observations and simulations reveals the inability of WRF to simulate turbulent structures. For simulations nudged towards reanalysis data (WRF-ERA) or forecasts (WRF-GFS) the characteristic lead times for WRF to acquire skills are given in Table 1. For simulations where WRF is nudged towards forecast data (WRF-GFS) skill will deteriorate for large lead times owing to the nonlinearity of the Navier-Stokes equations.

Both for wind speed and direction the skills start to decrease after ≈ 3 days.

Lack of skill in a forecast of wind speed corresponding to a correlation coefficient of 0.6 is found for a lead time larger than ≈ 6 days.

Similarly, lack of skill in a forecast of wind direction is found for a lead time larger than ≈ 4 days.

Even for a lead time of 8 days, there is some skill in the forecasted wind speed and direction (correlation coefficient ≈ 0.4).

Persistence, i.e. the simulated wind speed or direction ahead of time is equal to or better predicted than the conditions at the time of the forecast. For wind speed it is ≈ 2 hours for WRF-ERA and a little smaller, ≈ 1.5 hours for WRF-GFS, corresponding correlation coefficient between observations and simulations of ≈ 0.4. For the wind direction it is ≈ 1.5 hours for both WRF-ERA and WRF-GFS.

Often there is a time shift between model simulations and the observations (Haupt et al., 2014). The fraction of time that a phase shift in the model simulations improved the comparison with observations is illustrated. For a time shift of 2 hours, it is about ≈ 20 % of the time for the WRF-ERA simulations. For WRF-GFS simulations with a forecast horizon of 0.5 days it is also about ≈ 20 %; for an increasing forecast horizon the sensitivity of a time shift in the model simulations, when compared with observations, decreases.

It can be noted that in order to have perfect agreement between simulations and observations, the correlation coefficient must be one and the variance of the two distributions equal.

Acknowledgements

This study was supported by the Danish Council for Strategic Research, project number 2104-08-0025 named "Tall Wind" and the COST action ES1303 TOPROF. The meteorological measurements from the mast at the FINO3 research platform were kindly made available by the BMU (Bundesministerium für Umwelt, German Federal Ministry for the Environment, Nature Conservation and Nuclear Safety) and the PTJ (Projektträger Jülich, project executing organisation). We thank the BMU for allowing the installation and operation of the wind-lidar at FINO3, the Test and Measurements section of DTU Wind Energy for operation and maintenance of the database, and Kit Rackley and Paul Halton who kindly read through the manuscript.

References

Banks, R.F., J. Tiana-Alsina, J.M. Baldasano, F. Rocadenbosch, A. Papayannis, S. Solomos, C.G. Tzanis, 2016: Sensitivity of boundary-layer variables to PBL schemes in the WRF model based on surface meteorological observations, lidar, and radiosondes during the HygrA-CD campaign. – Atmos. Res. **176–177**, 185–201.

Bengtsson, L., J. Shukla, 1988: Integration of space and in situ observations to study global climate change. – Bull. Amer. Meteor. Soc. **69**, 1130–1143.

Boadh, R., A.N.V. Satyanarayana, T.V.B.P.S. Rama Krishna, S. Madala 2016: Sensitivity of PBL schemes of the WRF-ARW model in simulating the boundary layer flow parameters for its application to air pollution dispersion modeling over a tropical station. – Atmósfera **29**, 61–81.

Bollmeyer, C., J.D. Keller, C. Ohlwein, S. Bentzien, S. Crewell, P. Friederichs, A. Hense, J. Keune, S. Kneifel, I. Pscheidt, S. Redl, S. Steinke, 2015: Towards a high-resolution regional reanalysis for the European CORDEX domain. – Quart. J. Roy. Meteor. Soc. **141**, 1–15.

Borsche, M., A.K. Kaiser-Weiss, F. Kaspar, 2016: Wind speed variability between 10 and 116 m height from the regional reanalysis COSMO-REA6 compared to wind mast measurements over Northern Germany and the Netherlands. – Adv. Sci. Res. **13**, 151–161.

Brümmer, B., S.M. Schultze, 2015: Analysis of a 7-year low-level temperature inversion data set measured at the 280 m high Hamburg weather mast. – Meteorol. Z. **24**, 481–494.

Brümmer, B., I. Lange, H. Konow, 2012: Atmospheric boundary layer measurements at the 280 m high Hamburg weather mast 1995–2011: mean annual and diurnal cycles. – Meteorol. Z. **21**, 319–355.

Cariou, J.P. , 2013: Pulsed lidars. – In: Peña, A, C.B. Hasager, J. Lange, J. Anger, M. Badger, F. Bingöl, O. Bischoff, J.P. Cariou, F. Dunne, S. Emeis, M. Harris, M. Hofsäss, I. Karagali, J. Laks, S. Larsen, J. Mann, T. Mikkelsen, L.Y. Pao, M. Pitter, A. Rettenmeier, A. Sathe, F. Scanzani, D. Schlipf, E. Simley, C. Slinger, R. Wagner, I. Würth (Eds.): Remote sensing for wind energy. – DTU Wind Energy-E-Report-0029(EN), 104–121.

Carvalho, D., A. Rocha, M. Gómez-Gesteira, C. Silva Santos, 2014: Offshore wind energy resource simulation forced by different reanalyses: Comparison with observed data in the Iberian Peninsula. – Appl. Energy **134**, 57–64.

Chen, F., J. Dudhia, 2001: Coupling an advanced land surface-hydrology model with the Penn State-NCAR. MM5 modeling system. Part I: model implementation and sensitivity. – Mon. Wea. Rev. **129**, 569–585.

Collazo, S., O. Lhotka, M. Rusticucci, J. Kyselý, 2018: Capability of the SMHI-RCA4 RCM driven by the ERA-Interim reanalysis to simulate heat waves in Argentina. – Int. J. Climatol. **38**, 483–496.

Dee, D.P., S.M. Uppala, A., J. Simmons, P. Berrisford, P. Poli, S. Kobayashi, U. Andrae, M.A. Balmaseda, G. Balsamo, P. Bauer, P. Bechtold, A.C.M. Beljaars, L. van de Berg, J. Bidlot, N. Bormann, C. Delsol, R. Dragani, M. Fuentes, A.J. Geer, L. Haimberger, S.B. Healy, H. Hersbach, E.V. Hólm, L. Isaksen, P. Kållberg, M. Köhler, M. Matricardi, A.P. McNally, B.M. Monge-Sanz, J.-J. Morcrette, B.-K. Park, C. Peubey, P. de Rosnay, C. Tavolato, J.-N. Thépaut, F. Vitart, 2011: The ERA-Interim reanalysis: configuration and performance of the data assimilation system. – Quart. J. Roy. Meteor. Soc. **137**, 553–597.

Draxl, C., A.N. Hahmann, A. Peña, G. Giebel, 2014: Evaluating winds and vertical wind shear from Weather Research and Forecasting model forecasts using seven planetary boundary layer schemes. – Wind Energy **17**, 39–55.

Durante, F., A. Westerhellweg, 2012: A comparison of a mesoscale model with FINO measurements in the German Bight and the Baltic Sea. – DEWI Magazin, **40**, 67–72.

Floors, R., C.L. Vincent, S.E. Gryning, A. Peña, E. Batchvarova, 2013: The wind profile in the coastal boundary layer: wind lidar measurements and numerical modelling. – Bound.-Layer Meteor. **147**, 469–491.

Floors, R., A. Hahmann, A. Peña, 2018: Evaluating mesoscale simulations of the coastal flow using lidar measurements. – J. Geophys. Res. **123**, 2718–2736.

Frehlich, R. , 1996: Simulation of coherent Doppler lidar performance in the weak-signal regime. – J. Atmos. Oceanic. Technol. **13**, 646–658.

Gryning, S.E. , 1985: The Øresund Experiment-A Nordic Mesoscale Dispersion Experiment over a Land-Water-Land Area. – Bull. Amer. Meteor. Soc. **66**, 1403–1407.

Gryning, S. E, E. Batchvarova, 2002: Marine boundary layer and turbulent fluxes over the Baltic Sea: Measurements and modelling. – Bound.-Layer Meteor. **103**, 29–47.

Gryning, S.E., R. Floors, 2019: Carrier-to-Noise-Threshold Filtering on Off-Shore Wind Lidar Measurements. – Sensors **19**, 592.

Gryning, S.E., E. Batchvarova, B. Brümmer, H. Jørgensen, S. Larsen, 2007: On the extension of the wind profile over homogeneous terrain beyond the surface boundary layer. – Bound.-Layer Meteor. **124**, 251–268.

Gryning, S.E., E. Batchvarova, R. Floors, A. Peña, B. Brümmer, A.N. Hahmann, T. Mikkelsen, 2014: Long-term profiles of wind and Weibull distribution parameters up to 600 m in a rural coastal and an inland suburban area. – Bound.-Layer Meteor. **150**, 167–184.

Gryning, S.E., R. Floors, A. Peña, E. Batchvarova, B. Brümmer, 2016: Weibull Wind-Speed Distribution Parameters Derived from a Combination of Wind-Lidar and Tall-Mast Measurements Over Land, Coastal and Marine Sites. – Bound.-Layer Meteor. **159**, 329–348.

Haupt, S.E., W.P. Mahoney, K. Parks, 2014: Wind power forecasting. – In: Troccoli, A., L. Dubus, S.E. Haupt (Eds.): Weather matters for energy. – Springer Academic Publishers, Dordrecht, 292–318.

Hersbach, H., 2002: Decomposition of the continuous ranked probability score for ensemble prediction systems. – Wea. Forecast. **15**, 559-570.

Hersbach, H., D. Dee, 2016: ERA5 reanalysis is in production. – ECMWF Newsletter 147, 7.

Hollingworth, A. K, M. Arpe, M. Tiedtke, M. Capaldo, H. Savijaervi, 1980: The performance of a medium range forecast model in winter – impact of physical parameterizations. – Mon. Wea. Rev. **108**, 1736–1773.

Høyer, J.L., I. Karagali, 2016: Sea Surface temperature climate record for the North Sea and Baltic Sea. – J. Climate **29**, 2529–2541.

Jacob, D. , 2014: Development and validation of a coupled model system in the Baltic region – BALTIMOS. –Theor. Appl. Climatol. **118**, 09-610. DOI:10.1007/s00704-014-1291-z.

Lorenz, E., 1963: Deterministic nonperiodic flow. – J. Atmos. Sci. **20**,130–141.

Nielsen, T.S., A. Joensen, H. Madsen, L. Landberg, G. Giebel, 1998: A new reference for wind power forecasting. – Wind Energy **1**, 29–34.

Noh, Y., W.G. Cheon, S.Y. Hong, 2003: Improvement of the K-profile Model for the Planetary Boundary Layer based on Large Eddy Simulation Data. – Bound.-Layer Meteor. **107**, 401–427.

Parker, W.S. , 2016: Reanalyses and Observations: What's the Difference? – Bull.Amer. Meteor. Soc. **97**, 1565–1572.

Peña, A., S.E. Gryning, J. Mann, C.B. Hasager, 2010: Length Scales of the Neutral Wind Profile over Homogeneous Terrain. – Jour. Appl. Meteor. Climatol. **49**, 792–806.

Peña, A, R. Floors, A. Sathe, S.E. Gryning, R. Wagner, M.S. Courtney, X.G. Lársen, A.N. Hahmann, C.B. Hasager, 2015: Ten years of boundary-layer and wind-power meteorology at Høvsøre, Denmark. – Bound.-Layer Meteor. **158**, 1–26.

Pietikäinen, J.P., T. Markkanen, K. Sieck, D. Jacob, J. Korhonen, P. Räisänen, Y. Gao, J. Ahola, H. Korhonen, A. Laaksonen, J. Kaurola, 2018: The regional climate model REMO (v2015) coupled with the 1-D freshwater lake model FLake (v1): Fenno-Scandinavian climate and lakes. – Geosci. Model Dev. **11**, 1321–1342. DOI:10.5194/gmd-11-1321-2018.

Pinson, P. , 2012. Very-short-term probabilistic forecasting of wind power with generalized LogiteNormal distributions. – J. Roy. Stat. Soc. Series C (Applied Statistics) **61**, 555–576.

Pinson, P., L. Christensen, H. Madsen, E. Sørensen, M.H. Donovan, L.E. Jensen, 2008: Regime-switching modelling of the fluctuations of offshore wind generation. – J. Wind Engineer. Indust. Aerodyn. **96**, 2327–2347.

Rienecker, M.M., M.J. Suarez, R. Gelaro, R. Todling, J. Bacmeister, E. Liu, M.G. Bosilovich, S.D. Schubert, L. Takacs, G.K. Kim, S. Bloom, J. Chen, D. Collins, A. Conaty, A. da Silva, W. Gu, J. Joiner, R.D. Koster, R. Lucchesi, A. Molod, T. Owens, S. Pawson, P. Pegion, C.R. Redder, R. Reichle, F.R. Robertson, A.G. Ruddick, M. Sienkiewicz, J. Woollen, 2011: The Modern-Era Retrospective Analysis for Research and Applications, Version 2 (MERRA-2). – J. Climate **24**, 3624–3648.

Sathe, A., J. Mann, 2013: A review of turbulence measurements using ground-based wind lidars. – Atmos. Mea. Tech., **6**, 3147–3167.

Seity, Y., P. Brousseau, S. Malardel, G. Hello, P. Bénard, F. Bouttier, C. Lac, and V. Masson, 2011: The AROME-France Convective-Scale Operational Model. – Mon. Wea. Rev. **139**, 976–991.

Simmons, A.J., D.M. Burridge, 1981: An energy and angular-momentumconserving finite-difference scheme and hybrid coordinates. – Mon. Wea. Rev. **109**, 758–766.

Simon, W., D. Hassell, D. Hein, R. Jones, R. Taylor, 2004: Installing and Using the Hadley Centre Regional Climate Modelling System, PRECIS, Version 1.1. – Met Office Hadley Centre, Exeter.

Skamarock, W.C., J.B. Klemp, J. Dudhia, D.O. Gill, D.M. Barker, M.G. Duda, X.Y. Huang, W. Wang, J.G. Powers, 2008: A description of the advanced research. WRF version 3. NCAR/TN-475+STR. – NCAR technical note, Mesoscale and Microscale Meteorology Division, National Center for Atmospheric Research, Boulder, 113 pp

Steyn, D.G., I.G. McKendry, 1988: Quantitative and qualitative evaluation of a three-dimensional mesoscale numerical model simulation of a sea breeze in complex terrain. – Mon. Wea. Rev. **116**, 1914–1926.

Suomi, I., S.E. Gryning, R. Floors, T. Vihma, C. Fortelius, 2015: On the vertical structure of wind gusts. – Quart. J Roy. Meteor. Soc. **141**, 1658–1670.

Suomi, I., S.E. Gryning, E.J. O'Connor, T. Vihma, 2017: Methodology for obtaining wind gusts using Doppler lidar. – Quart. J Roy. Met. Soc. **143**, 2061–2072.

Thompson, G., R.M. Rasmussen, K. Manning, 2004: Explicit forecasts of winter precipitation using an improved bulk microphysics scheme, part I: description and sensitivity analysis. – Mon. Wea. Rev. **132**, 519–542.

Troen, I., E. Petersen, 1989: European Wind Atlas. – Published for the European Commission DGXII by Risø National Laboratory. Denmark. 656 pp. ISBN 87-550-1482-8.

Van Ulden, A.P., J. Wieringa, 1996: Atmospheric boundary layer research at Cabauw. – Bound.-Layer Meteor. **78**, 39–69.

Vincent, C.L., P. Trombe, 2017: Forecasting intrahourly variability of wind generation. – In: Kariniotakis, G. (Ed.): Renewable Energy Forecasting, From Models to Applications. – Woodhead Publishing Series in Energy, 219–233.

Wyngaard, J.C. , 2010: Turbulence in the atmosphere. – Cambridge University Press, Cambridge, 393 pp.

Zhang, D., R.A. Anthes, 1982: A High-Resolution Model of the Planetary Boundary Layer – Sensitivity Tests and Comparisons with SESAME-79 Data. – J. Appl. Meteor. **21**, 1594–1609.